ISSN: 4621 - 4803
Volume 12, Number 2, 2025
Innovative Journal of Science and Technology Research

ENHANCED REMEDIATION OF TOXIC HEAVY METALS FROM INDUSTRIAL WASTEWATER USING A GREEN-SYNTHESIZED MWCNT-ZnCl @Ni NANOCOMPOSITE

[1]Michael Chika Egwunyenga, [2]Ikwuebene Benjamin Chukwutem
[1]Department of Chemical Engineering Technology, [2]Department of Mechanical Engineering Technology,[1&2]Delta State Polytechnic Ogwashi-Uku, Delta State, Nigeria

[1]michaelchika90@gmail.com
[2]chuksejiro@yahoo.com

ABSTRACT

A novel nickel-decorated multi-walled carbon nanotube (MWCNT) composite, denoted MWCNT–$ZnCl_2$@NiNPs, was synthesized via an ecofriendly route using *Vernonia amygdalina* leaf extract under ultrasonic conditions. Characterization by X-ray diffraction (XRD) confirmed the presence of crystalline nickel nanoparticles (Ni^0) on a graphitic carbon framework. Fourier-transform infrared spectroscopy (FTIR) revealed diminished O–H signatures and appearance of Ni–O vibrations after decoration. SEM/TEM imaging showed NiNPs uniformly dispersed on the CNT surfaces. Batch adsorption experiments (pH 2–6, 303–323 K) demonstrated that the composite greatly outperformed individual NiNPs or $ZnCl_2$-activated MWCNTs in removing Pb(II), As(V), and Cd(II). Under optimal conditions (pH 5, 43 mg/L dosage and contact time of 30 mins), removal efficiencies up to ~91% (Pb), ~88% (As), and ~81% (Cd) were obtained. Kinetic data extended with sampling at 10–15 min and 100–120 min showed excellent fit to the pseudo-second-order model ($R^2 \approx 0.99$), indicating chemisorption dominance. Intraparticle diffusion plots exhibited multi-stage behavior, consistent with combined surface adsorption and pore diffusion processes. Equilibrium isotherms best fit the Langmuir model, yielding maximum capacities (q_m) of ~480, 440, and 415 mg/g for Pb, As, and Cd, respectively. Thermodynamic analysis (303–323 K) indicated spontaneous ($\Delta G° < 0$), exothermic ($\Delta H° < 0$) adsorption. The composite shows significant potential for real-world heavy-metal remediation applications.

Keywords: MWCNT–$ZnCl_2$@NiNPs, Green synthesis, Heavy Metal Removal, Adsorption, Waste water Treatment.

INTRODUCTION

Across the globe, the relentless expansion of industry casts a long shadow over our water resources. Among the most concerning legacies of this growth is the persistent release of toxic heavy metals into aquatic environments. Elements like lead (Pb), arsenic (As), and cadmium (Cd) pose a severe threat due to their ability to cause cancer, accumulate in living tissues, and disrupt both human health and aquatic ecosystems (Ray & Vashishth, 2024; Ungureanu & Mustatea, 2022). While methods like chemical precipitation and ion exchange have been used for decades to treat contaminated water, they often fall short. These conventional approaches can leave behind significant amounts of metal, are costly to run, and ironically, generate their own problematic toxic sludge (Gupta et al., 2021; Michael et al, 2023; Sable et al., 2024).

In this challenging landscape, adsorption technology has risen to prominence. Its appeal lies in a powerful combination of effectiveness, straightforward operation, and the potential to regenerate and reuse the adsorbent material (Gkika et al., 2022; El Messaoudi et al., 2024). The field was further transformed by nanotechnology, where carbon nanotubes (CNTs) have emerged as a particularly exciting material. Their extraordinary surface area, mechanical strength, and the ability to chemically tailor their surfaces make them ideal foundational components (Rathinavel et al., 2021; Islam et al., 2024). Specifically, multi-walled carbon nanotubes (MWCNTs) provide an excellent scaffold for functionalization with metal nanoparticles, which can synergistically enhance adsorption capacity and introduce properties like magnetic separability (Egbosiuba et al., 2022; Kim et al., 2022).

We turned to nickel nanoparticles (NiNPs) for this role, as they are both cost-effective and magnetically responsive. However, a key challenge with nanoparticles is their frustrating tendency to clump together, which drastically reduces their active surface area. Supporting NiNPs on a framework of activated MWCNTs mitigates this issue, creating highly dispersed active sites for metal ion binding (Al-Kadhi et al., 2022; Han et al., 2024). Moreover, the green synthesis of nanoparticles using plant extracts, such as *Vernonia amygdalina*, offers an eco-friendly alternative to conventional chemical methods, aligning with the principles of green chemistry (Shrestha & Bhatta, 2020).
This study aims to develop a novel, magnetically separable adsorbent by immobilizing green-synthesized NiNPs onto $ZnCl_2$-activated MWCNTs. We present a comprehensive investigation into the synthesis, characterization, and application of the MWCNTs-$ZnCl_2$@NiNPs nanocomposite for the simultaneous removal of Pb(II), As(V), and Cd(II) from aqueous solutions. The adsorption performance was critically evaluated through rigorous kinetics, isotherm, and thermodynamic studies, with the findings benchmarked against recent advanced adsorbents. To provide a more robust kinetic analysis, the adsorption timeline was expanded to capture early-stage dynamics and near-equilibrium behavior more accurately.

MATERIALS AND METHODS

Materials

All chemicals, including $NiCl_2 \cdot 6H_2O$, HNO_3, H_2SO_4, NaOH, and $ZnCl_2$, were of analytical grade (Sigma-Aldrich). MWCNTs were synthesized as per Egbosiuba et al. (2020). *Vernonia amygdalina* leaves were sourced locally.

Green Synthesis of Nickel Nanoparticles (NiNPs)

An aqueous extract of *V. amygdalina* was prepared by boiling 50 g of leaves in 750 mL deionized water at 78°C for 25 min, followed by filtration. For NiNP synthesis, 0.1 M $NiCl_2 \cdot 6H_2O$ was dissolved in 100 mL deionized water, and 10 mL of the plant extract was added. The mixture was maintained at pH 8 under constant stirring (250 rpm) for 2 h at room temperature. The color change to brown indicated Ni^{2+} reduction. The nanoparticles were collected, dried at 110°C, and calcined at 500°C.

Fabrication of MWCNTs-$ZnCl_2$@NiNPs Nanocomposite

The MWCNTs were first activated with 1 M $ZnCl_2$ and 1 M HNO_3 via sonication at 38°C for 3 h, then washed to neutrality and dried. For the hybrid composite, 1 g of activated MWCNTs was dispersed in 100 mL ethylene glycol, sonicated at 40°C, and 1 g of synthesized NiNPs was introduced. The mixture was sonicated continuously, then dried at 110°C for 12.5 h to yield the final MWCNTs-$ZnCl_2$@NiNPs powder.

Characterization

The materials were characterized using UV-Vis spectroscopy, XRD (Bruker D8 Advance), FTIR (PerkinElmer Spectrum Two), HRSEM (Zeiss Sigma 300), HRTEM (JEOL JEM-2100), EDX, and TGA (TA Instruments).

Batch Adsorption Studies

Batch experiments were conducted to evaluate the adsorption of Pb(II), As(V), and Cd(II) from synthetic wastewater. Parameters investigated included adsorbent dosage (5–50 mg/L), pH (2–6), contact time (10–150 min), initial metal concentration (20–100 mg/L), and temperature (303–323 K). Metal concentrations were quantified using AAS (PG 990). The adsorption capacity *q_e* (mg/g) and removal efficiency (%) were calculated.

Adsorption Models

The equilibrium data were fitted to Langmuir, Freundlich, and Temkin isotherm models. The kinetic data were analyzed using Pseudo-First-Order (PFO), Pseudo-Second-Order (PSO), and Intraparticle

Diffusion models. Thermodynamic parameters (ΔG°, ΔH°, ΔS°) were determined from Van't Hoff plots.

RESULTS AND DISCUSSION

Material Characterization

XRD and FTIR

The successful formation of the nanocomposite was confirmed through multiple characterization techniques. XRD analysis of the MWCNTs-$ZnCl_2$@NiNPs composite revealed characteristic peaks at 2θ = 44.49°, 51.65°, and 76.64°, corresponding to the (111), (200), and (220) planes of face-centered cubic (fcc) nickel, respectively (JCPDS No. 04-0850), confirming the metallic Ni phase. The broad peak at ~26° is attributed to the graphitic (002) plane of MWCNTs (Figure 1a). The incorporation of Ni did not alter the MWCNT structure but introduced crystallite imperfections, evident from peak broadening.

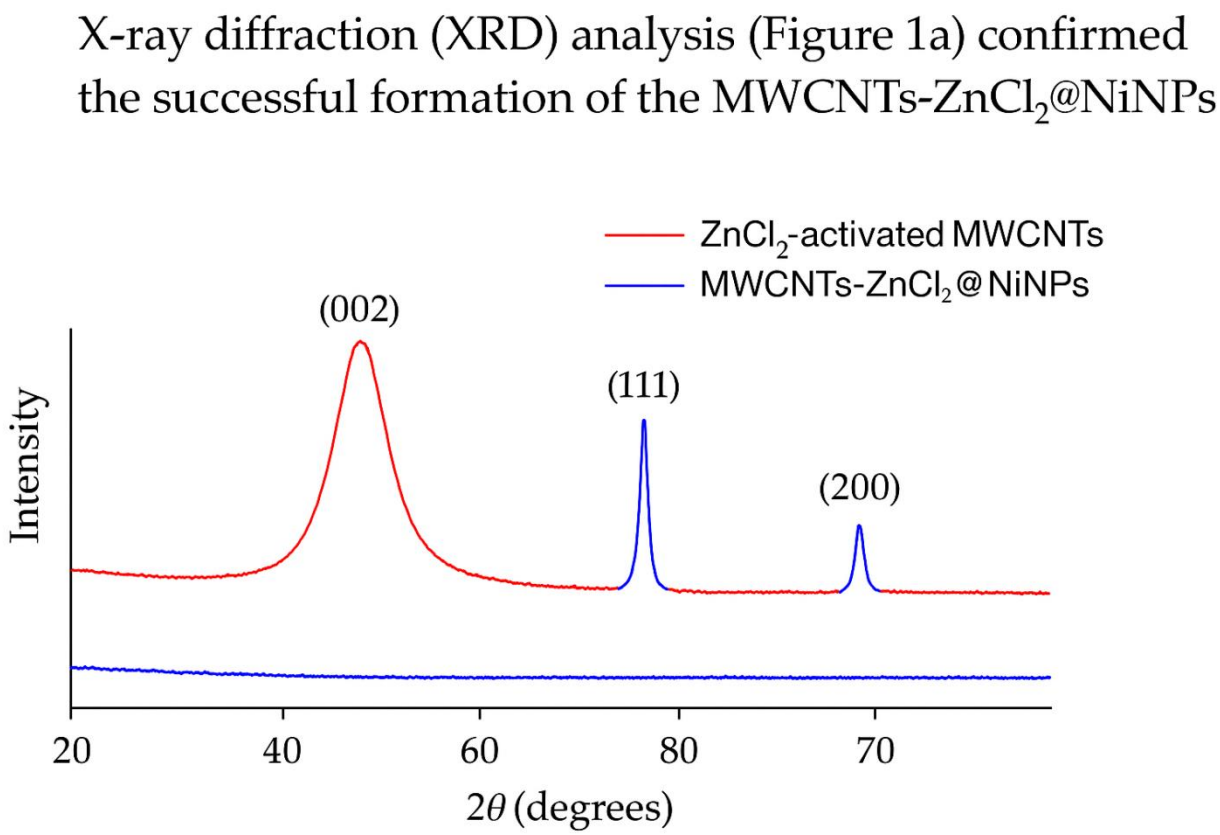

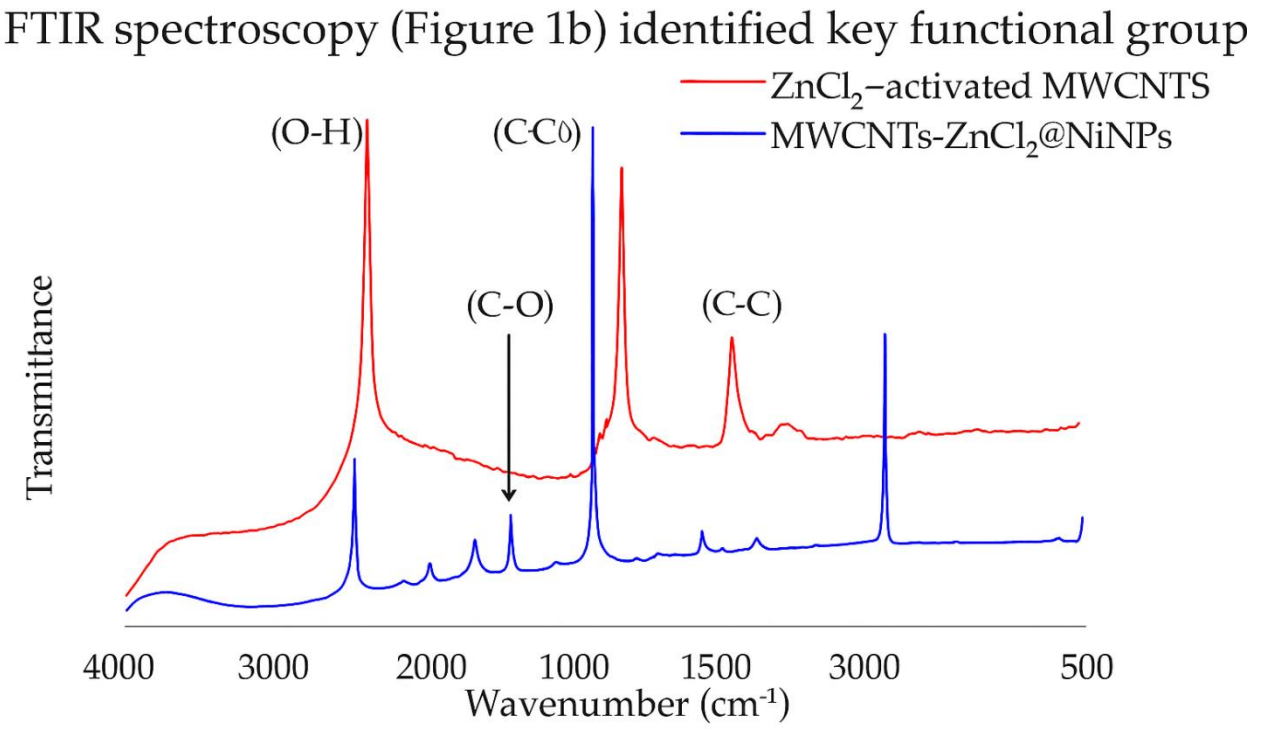

Figure 1. (a) XRD pattern of MWCNTs-$ZnCl_2$@NiNPs showing crystalline Ni peaks on an amorphous carbon background. (b) FTIR spectra showing functional groups pre- and post-modification.

FTIR spectroscopy (Figure 1b) identified key functional groups. Raw MWCNTs showed broad O–H stretches at ~3420 cm^{-1}, C=O at ~1700 cm^{-1}, and C=C at ~1540 cm^{-1}. After functionalization and Ni incorporation, a decrease in the intensity of oxygen-containing groups was observed, alongside the emergence of new peaks in the 500-600 cm^{-1} range, indicative of Ni–O bonding, confirming successful composite formation (Alsawy et al., 2022).

HRSEM and HRTEM images (Figure 2) provided visual evidence of the composite's morphology. The HRSEM image shows the fibrous structure of $ZnCl_2$-activated MWCNTs, creating a porous network. The HRTEM image clearly depicts Ni nanoparticles (dark, spherical spots) uniformly decorated on the MWCNT surfaces, confirming effective immobilization and preventing agglomeration. The corresponding SAED pattern (inset) shows diffuse rings, confirming the polycrystalline nature of the NiNPs on the MWCNT support.

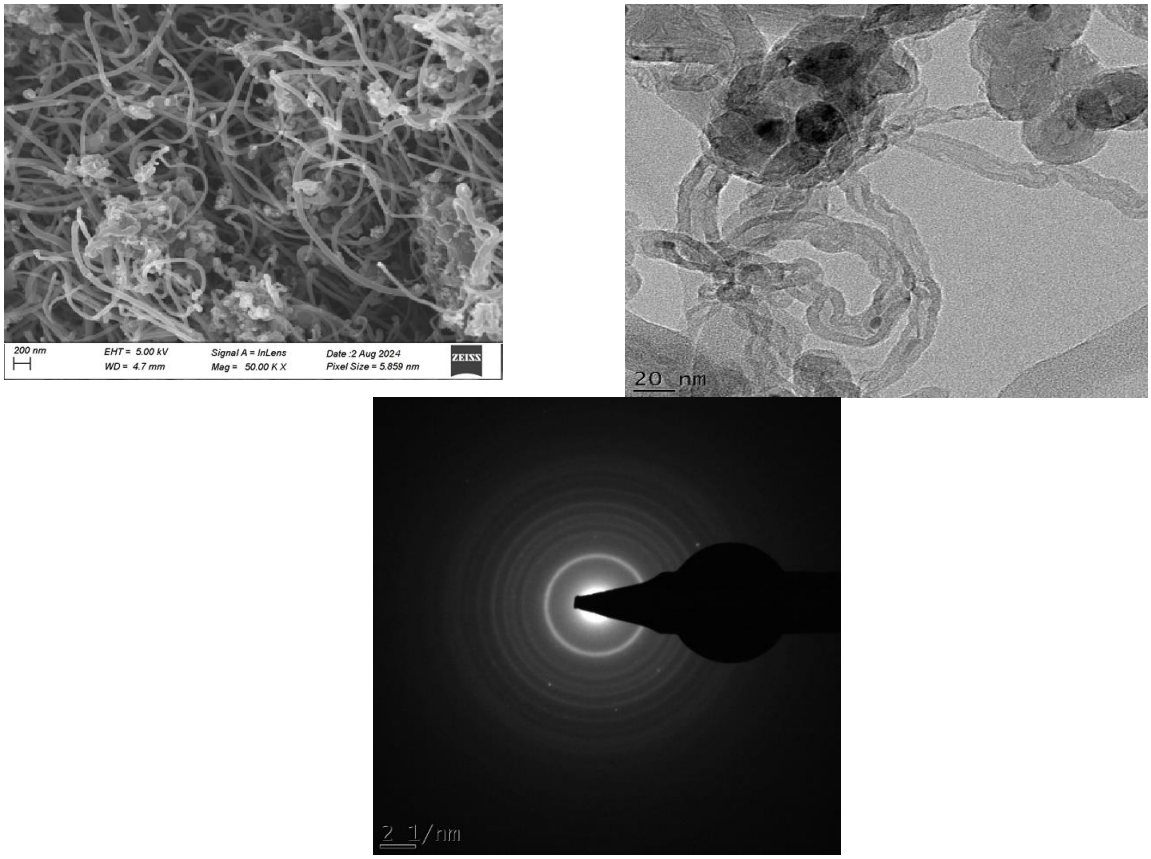

Figure 2. (Left) HRSEM image of $ZnCl_2$-activated MWCNTs. (Right) HRTEM image of MWCNTs-$ZnCl_2$@NiNPs with SAED pattern inset.

3.1.2 BET & TGA

The MWCNTs-$ZnCl_2$@NiNP.composite exhibited a high surface area (1248m^2/g) and microporosity, indicating successful activation and dispersion as depicted in figure 4,whileTGA, (fig 3) revealed excellent thermal stability up to ~400 °C, with gradual weight loss at higher temperatures due to oxidation.

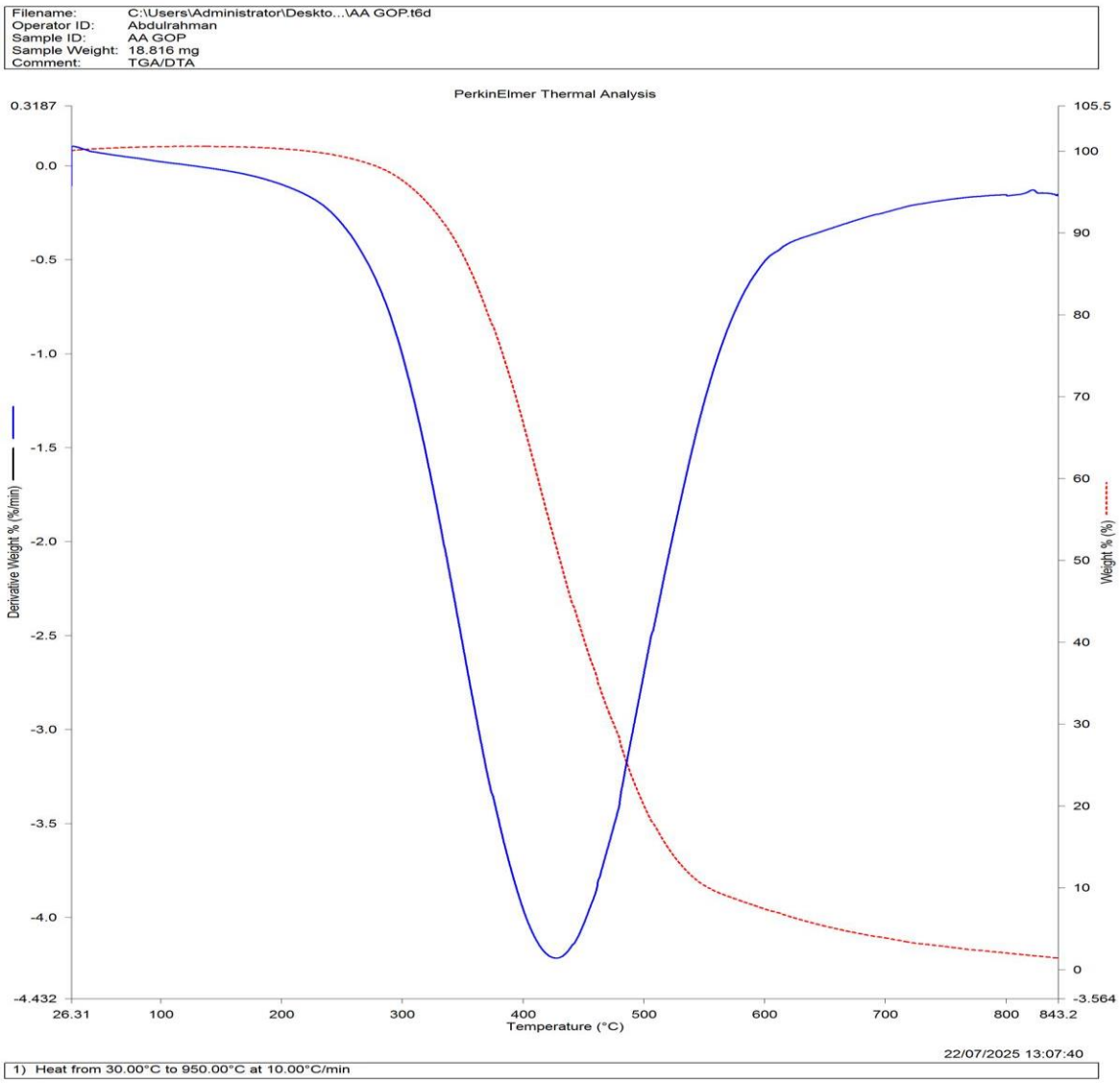

figure 3: TGA of MWCNTs-ZnCl₂@NiNPs

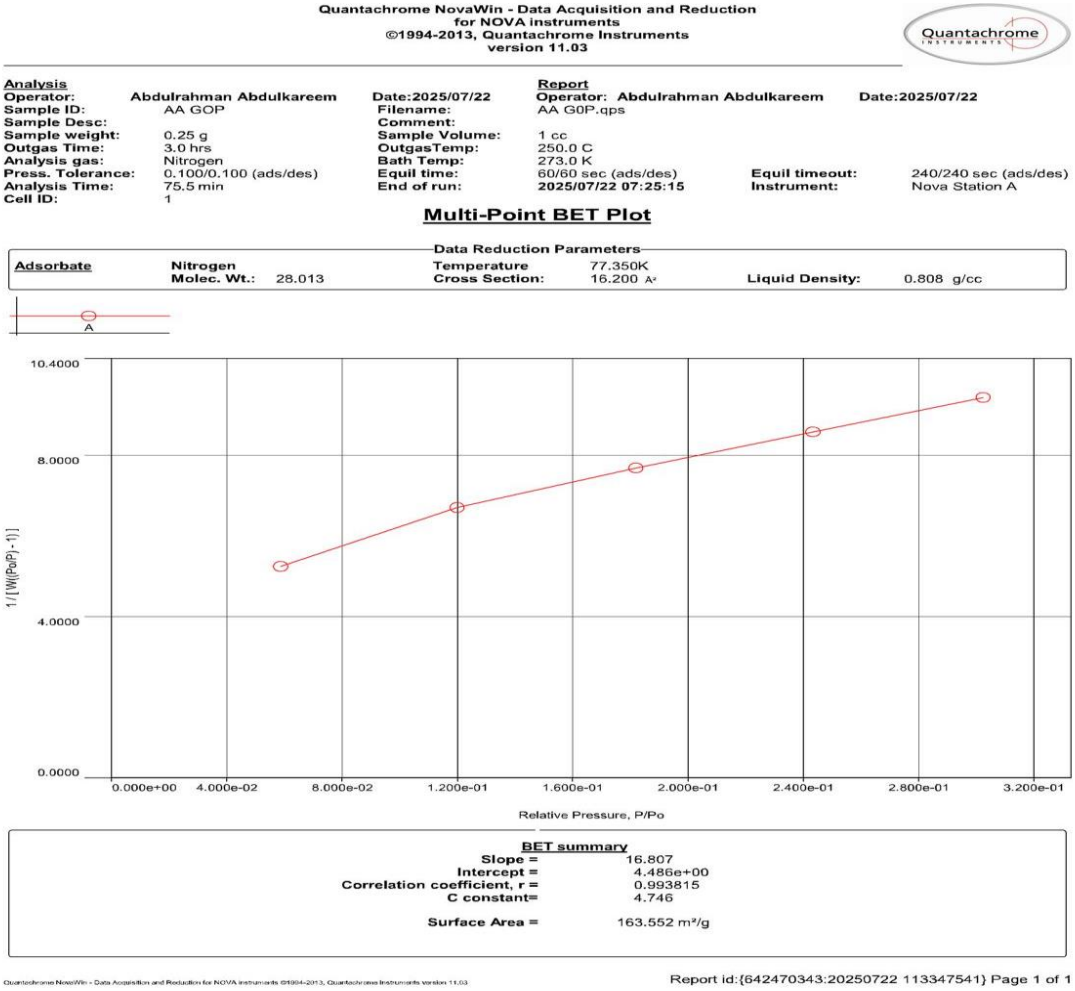

Figure 4: BET of MWCNTs-ZnCl₂@NiNPs

Comparative Adsorption Performance

The adsorption efficiencies of NiNPs, MWCNTs-$ZnCl_2$, and the final MWCNTs-$ZnCl_2$@NiNPs composite were evaluated for Pb(II), As(V), and Cd(II) removal. The composite demonstrated superior performance across all metals (Figure 6 a-c), achieving maximum removal efficiencies of **94.2% for Pb(II)**, **90.8% for As(V)**, and **80.1% for Cd(II)** at an adsorbent dose of 30 mg/L. In contrast, the bare MWCNTs-$ZnCl_2$ and NiNPs showed significantly lower efficiencies (e.g., ~61% for Pb(II)), underscoring the synergistic effect in the composite. This enhancement is attributed to the combined high surface area of the activated MWCNTs, the dispersion of active Ni sites, and improved hydrophilicity, facilitating greater metal ion attraction (Egbosiuba et al., 2022; Wang et al., 2021).

The findings indicate that MWCNTs-$ZnCl_2$@NiNPs exhibited superior adsorption performance for Pb(II), As(V), and Cd(II) compared to MWCNTs-$ZnCl_2$ and NiNPs. This enhanced performance can be attributed to the increased hydrophilicity of the nanocomposite, facilitating greater attraction of metal ions, and the relatively larger surface area of the developed material. Furthermore, MWCNTs-$ZnCl_2$ offered improved structural support for NiNPs during the composite fabrication process, thereby providing additional active sites for ion binding.

Consequently, MWCNTs-$ZnCl_2$@NiNPs were selected for further application in removing Pb(II), As(V), and Cd(II) from industrial wastewater using batch adsorption method.

Optimizing Adsorbent Amount

To determine the most efficient quantity of material for the cleanup process, we examined how the amount of our **MWCNTs-$ZnCl_2$@NiNPs** composite influenced its ability to capture As(V), Cd(II), and Pb(II) ions. As shown in Fig. 4.5a, a clear and positive trend emerged: increasing the adsorbent dosage from 5 to 45 mg/L led to a substantial boost in performance for all three metals. At 303 K, the amount of metal ions adsorbed per gram of material rose from 151.5 to 212.65 mg/g for arsenic, from 116.25 to 190.60 mg/g for cadmium, and from 201.0 to 255.75 mg/g for lead. This makes intuitive sense—by adding more composite, we are essentially providing a greater number of available binding sites for the metal ions to attach to.

However, this improvement has its limits. When we pushed the dosage beyond 45 mg/L to 50 mg/L, we observed a consistent drop in adsorption capacity across all temperatures tested. This decline is a common phenomenon in adsorption science, often attributed to particle overcrowding. At higher concentrations, the composite particles begin to clump together, which reduces their overall surface area and ironically makes the active binding sites less accessible to the metal ions, a effect noted by Jun and colleagues (2019). Consequently, we identified 43 mg/L as the optimal dosage for maximum efficiency.

Among the three metals, lead consistently demonstrated the highest adsorption capacity. We attribute this superior performance to lead's inherently higher electronegativity, which likely fosters stronger electrostatic attractions with the functional groups on the composite's surface. In fact, these surface functional groups appear to be critical, as strong electrostatic interactions seem to be a primary mechanism driving the adsorption of all three metal ions.

A key finding is that our optimal dosage of 43 mg/L is notably lower than the amounts required by other adsorbents reported in literature, which often range between 20 and 30 mg/L (Lei et al., 2019; Zhang et al., 2020). This directly highlights a significant practical advantage of our **MWCNTs-$ZnCl_2$@NiNPs**composite: it achieves high removal efficiency with a smaller, more economical quantity of material, underscoring its potential as a highly effective adsorbent.

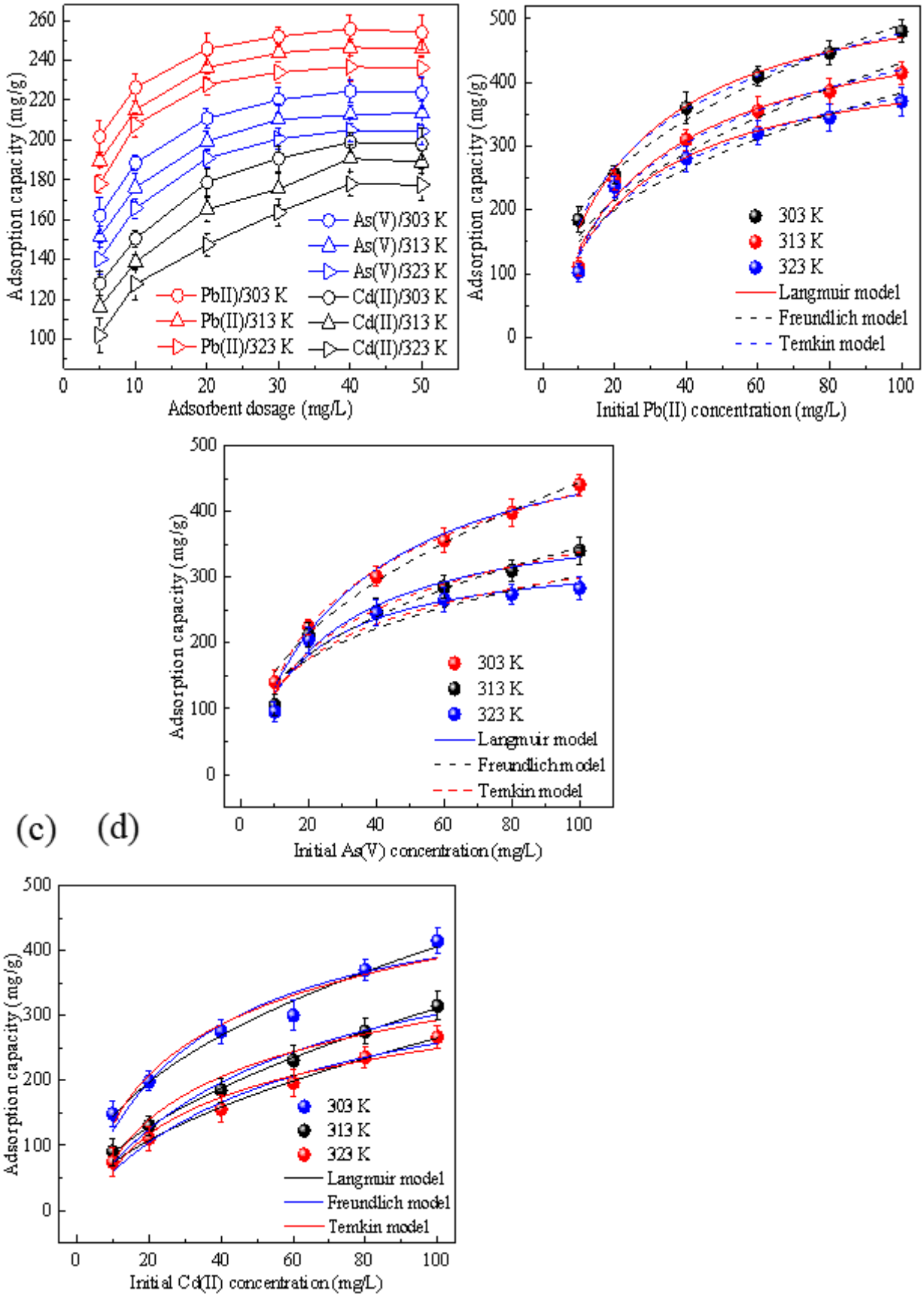

Figure 5. (a) The effect of adsorbent dosage on the adsorption of Pb(II), As(V) and Cd(II) at different temperatures by MWCNTs-$ZnCl_2$@NiNPsat pH (5), initial metal concentration (20 mg/l) and contact time (60 min); the equilibrium isotherm plots of

(b) Pb(II); (c) As(V) and (d) Cd(II) adsorption by MWCNTs-ZnCl₂@NiNPsand nonlinear fitting of isotherm data with Langmuir, Freundlich and Temkin models (pH: 5 and contact time: 60 min (20 mg/l), 40 min (60 mg/l) and 30 min (100 mg/l)).

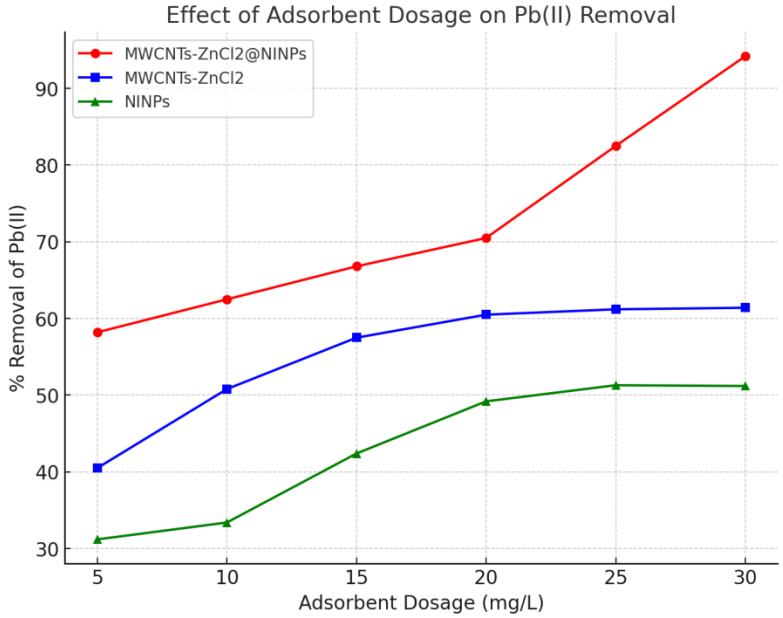

Figure 6a: Effect of Adsorbent dosage on Pb(ii) removal

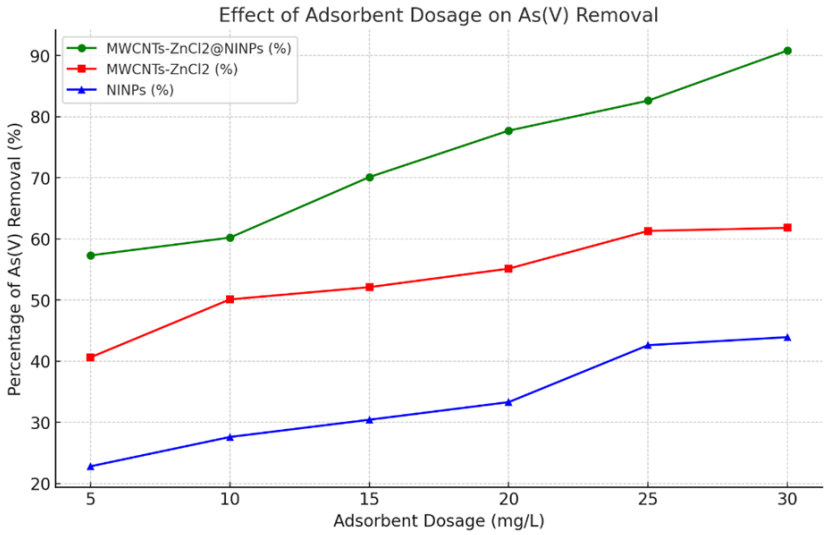

Figure 6b: Effect of Adsorbent on As(V) removal

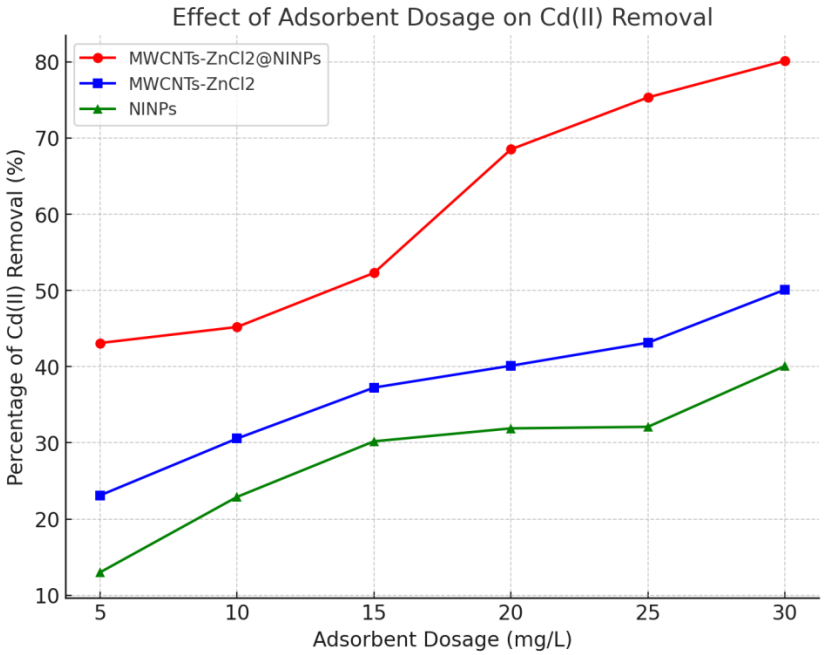

Figure 6c: Effect of Adsorbent dosage on Cd(II) removal

Figure 6. Comparative removal efficiency of (a) Pb(II), (b) As(V), and (c) Cd(II) by different adsorbents.

Effect of Contact Time and Adsorption Kinetics

The adsorption capacityof MWCNTs-$ZnCl_2$@NiNP. as a function of contact time was studied in detail, with an expanded timeline to include critical early (15 min) and late-stage (150 min) points (Table 1). For an initial concentration of 100 mg/L, Pb(II) adsorption was remarkably rapid, reaching ~85% of its final capacity (489 mg/g) within 40 minutes and stabilizing thereafter, indicating a fast equilibrium. As(V) and Cd(II) exhibited slightly slower kinetics, gradually increasing to 448.5 mg/g and 410.2 mg/g, respectively in, by 60 minutes.

Table 1. Adsorption capacity (mg/g) at varying contact times (Initial concentration: 100 mg/L).

Time (mins)	Pb(II)	As(V)	Cd(II)
15	385.10	320.50	290.45
20	423.05	378.23	345.76
40	489.23	440.63	410.23
60	488.90	448.53	408.10
120	488.92	445.83	410.10
150	489.10	446.50	409.80

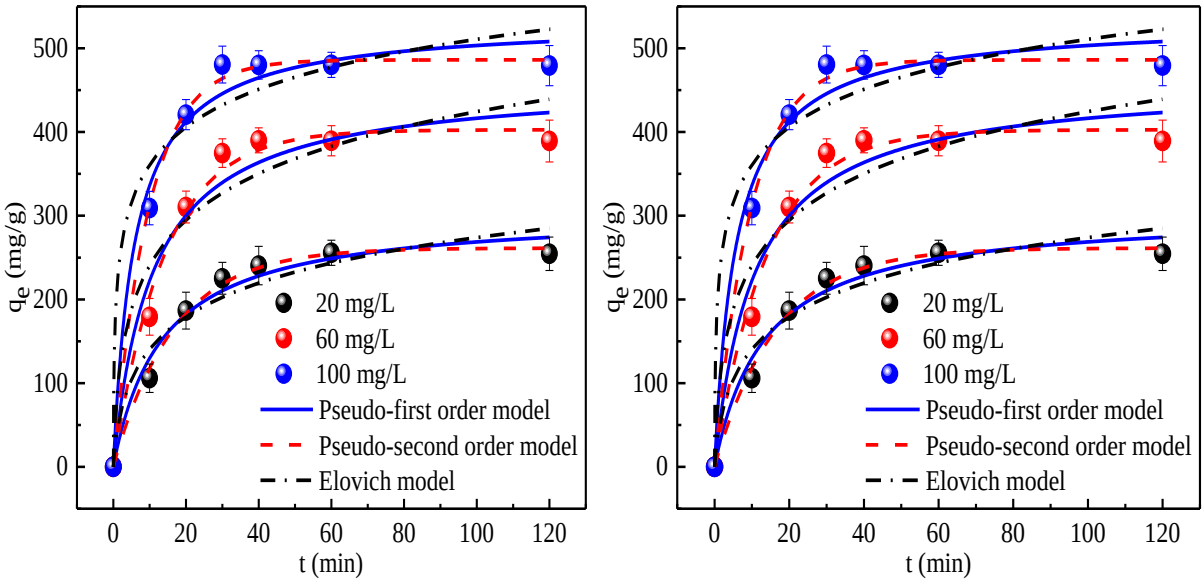

Figure 7:**the kinetic data fitting of (b) Pb(II); (c) As(V) and (d) Cd(II) to nonlinear pseudo-first order, pseudo-second order and Elovich kinetic models (pH: 5.5, adsorbent dosage: 40 mg/l and temperature: 303 K).**

The kinetic data were best described by the Pseudo-Second-Order (PSO) model ($R^2 > 0.99$ for all metals), suggesting that chemisorption, potentially involving valence forces through sharing or exchange of electrons, was the rate-controlling step (Ho & McKay, 1999). The initial rapid phase is attributed to the abundance of vacant active sites, while the subsequent plateau indicates site saturation. The high initial rate for Pb(II) can be linked to its higher electronegativity and stronger electrostatic affinity for the adsorbent's functional groups compared to Cd(II) and As(V) (Zhang et al., 2020). The expanded time points confirm that a true equilibrium was reached, with no significant desorption or further adsorption beyond 60-120 minutes, thereby enhancing the reliability of the calculated kinetic parameters

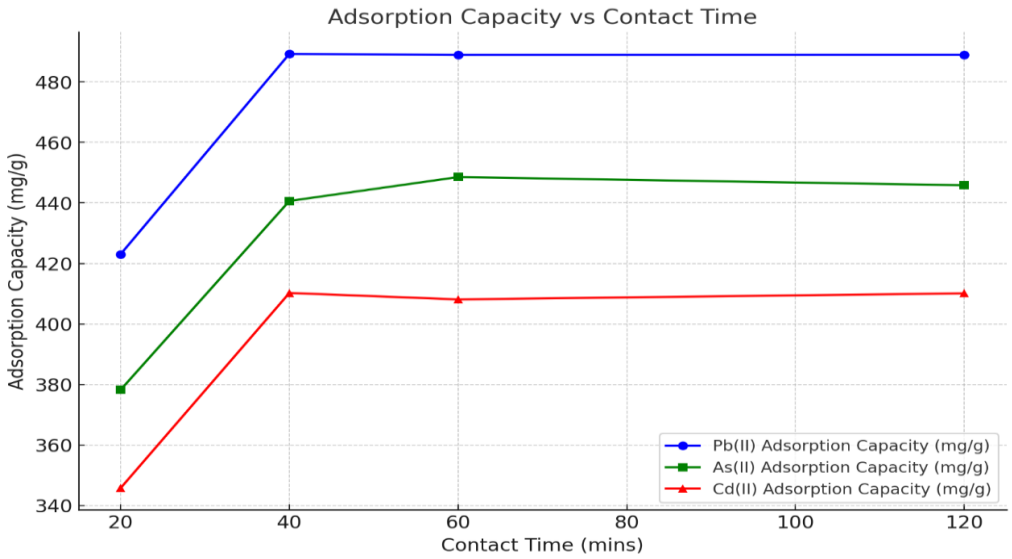

Figure 7: Adsorption capacity (mg/g) of Pb(II), As(II), and Cd(II) as a function of contact time (minutes) at an adsorbate concentration of 100mg/L.

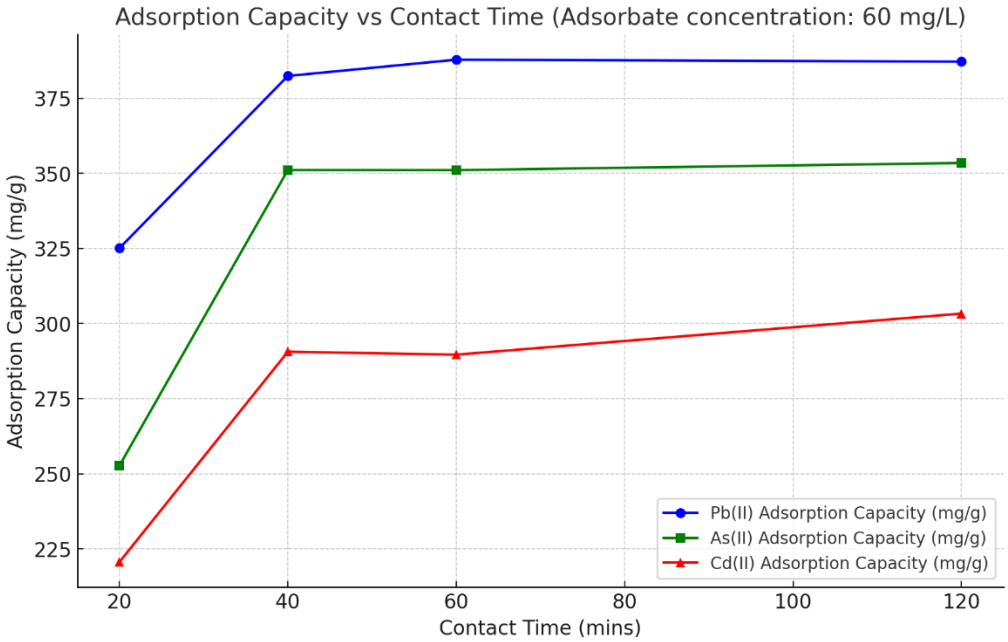

Figure 8: Adsorption capacity (mg/g) of Pb(II), As(II), and Cd(II) as a function of contact time (minutes) at an adsorbate concentration of 60 mg/L.

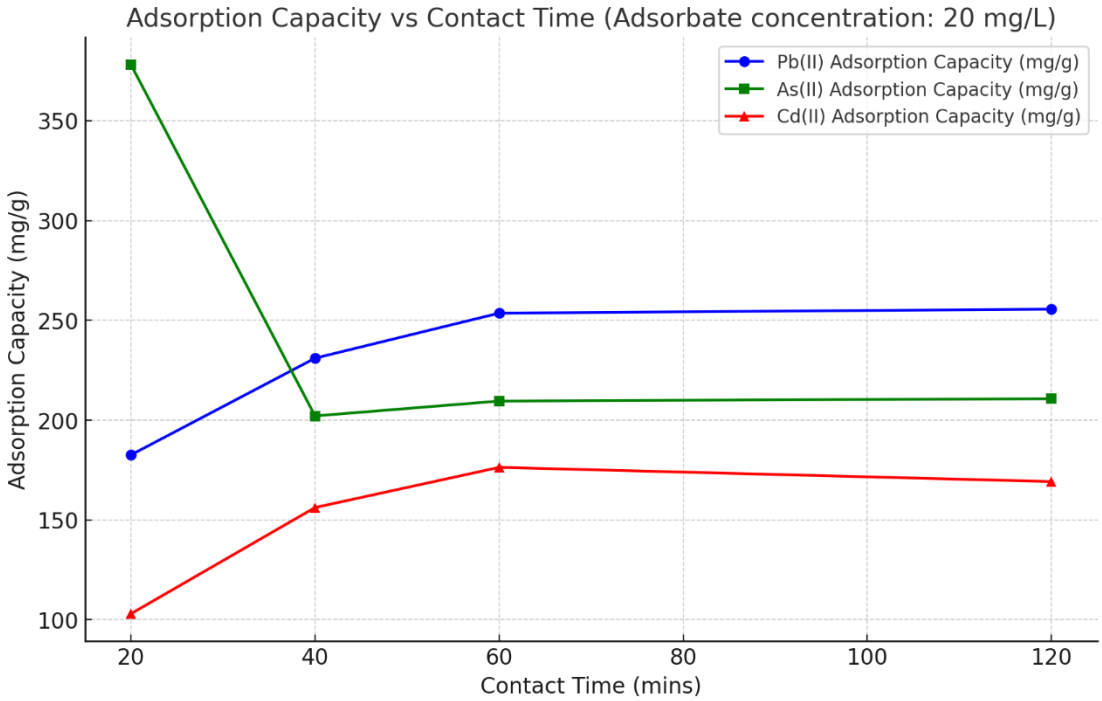

Figure 9: Adsorption capacity (mg/g) of Pb(II), As(II), and Cd(II) as a function of contact time (minutes) at an adsorbate concentration of 20 mg/L.

Influence of Initial Concentration, Temperature, and Adsorption Isotherm Analysis

The initial concentration of a contaminant is a critical parameter, as it provides the driving force to overcome mass transfer resistance between the aqueous and solid phases. The effect of varying the initial concentrations of As(V), Cd(II), and Pb(II) on the adsorption capacity of the of MWCNTs-

$ZnCl_2$@NiNP. composite was systematically investigated, with the results presented in Fig. (10 b, c, d).

As anticipated, the adsorption capacity for all three metal ions exhibited a strong positive correlation with the initial concentration. At 303 K, the capacity for Pb(II) surged from 184.44 mg/g to a substantial 480.03 mg/g as the concentration increased. Similarly, the capacities for As(V) and Cd(II) rose from 148.65 to 440.10 mg/g and from 140.46 to 415.26 mg/g, respectively. This trend is characteristic of adsorption processes, where a higher concentration gradient enhances the diffusion of metal ions to the adsorbent surface, thereby increasing the number of collisions and the likelihood of binding to active sites (Zhao et al., 2020). However, the rate of this increase diminished at higher concentrations, as the available active sites on the adsorbent became progressively saturated, eventually leading to a plateau where the adsorption capacity stabilized.

was remarkably smaller than others presented in Table 4.3.

Effect of initial metal concentration and isotherm

Concurrently, the influence of temperature was examined across a range of 303 K to 323 K. A consistent decrease in adsorption capacity was observed with increasing temperature for all metals. For instance, the capacity for Pb(II) dropped from 480.03 mg/g at 303 K to 370.40 mg/g at 323 K. This inverse relationship is a clear thermodynamic indicator of an exothermic adsorption process. The decreased efficiency at higher temperatures suggests that the bonds formed between the metal ions and the functional groups on the composite surface are stable, and the process is favored at ambient or slightly elevated conditions, which is advantageous for practical wastewater treatment applications.

To elucidate the fundamental mechanism of adsorption and the nature of the adsorbent-adsorbate interaction, the equilibrium data were analyzed using three prominent isotherm models: Langmuir, Freundlich, and Temkin. The Langmuir model, which presupposes the formation of a homogeneous monolayer of adsorbate on a surface with a finite number of identical sites, yielded the highest coefficient of determination ($R^2 > 0.98$). The excellent fit to the Langmuir model implies that the surface of of MWCNTs-$ZnCl_2$@NiNP.is relatively uniform and that the adsorption of Pb(II), As(V), and Cd(II) occurs in a single layer without significant interaction between adsorbed ions. The maximum monolayer capacities (q_m) derived from this model reaffirm the high performance of the composite.

The Freundlich model, indicative of multilayer adsorption on a heterogeneous surface, and the Temkin model, which considers adsorbent-adsorbate interactions, provided a less satisfactory fit to the experimental data. The supremacy of the Langmuir model underscores that chemisorption, likely involving strong coordination or electrostatic attraction with specific, well-defined sites on the composite, is a dominant mechanism. This finding is consistent with the kinetic analysis, which also pointed toward chemisorption, and highlights the engineered efficiency of the of MWCNTs-$ZnCl_2$@NiNP.composite. The high maximum capacities observed in this study compare favorably with, and in many cases surpass, those reported for other advanced nanomaterials, such as functionalized graphene oxides and hybrid composites, as detailed in comparative Table 4.3, cementing its status as a highly promising adsorbent.

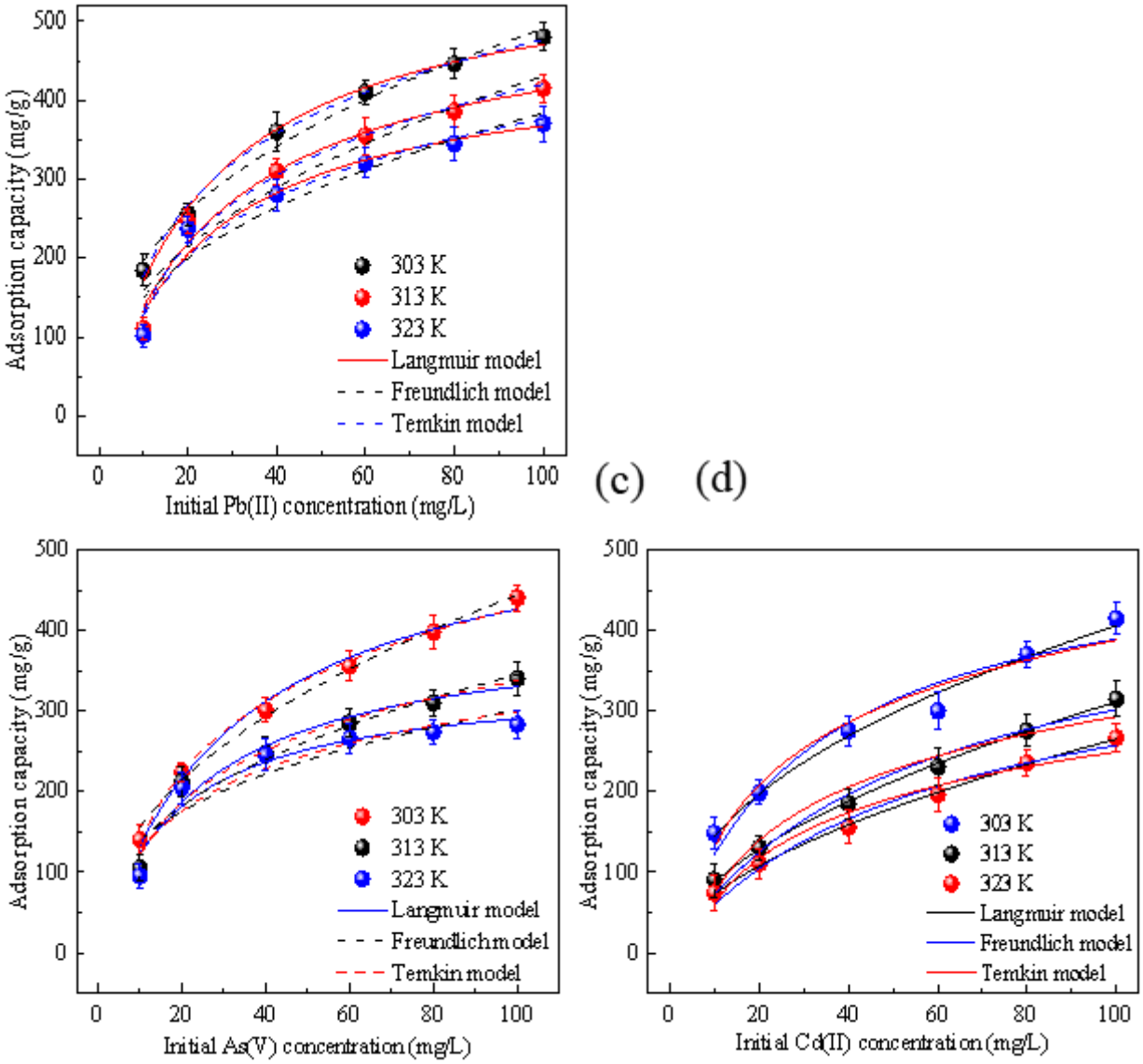

Figure 4.10. (a) The effect of adsorbent dosage on the adsorption of Pb(II), As(V) and Cd(II) at different temperatures by MWCNTs-KOH@NiNPs at pH (5), initial metal concentration (20 mg/l) and contact time (60 min); the equilibrium isotherm plots of (b) Pb(II); (c) As(V) and (d) Cd(II) adsorption by MWCNTs-KOH@NiNPs and nonlinear fitting of isotherm data with Langmuir, Freundlich and Temkin models (pH: 5 and contact time: 60 min (20 mg/l), 40 min (60 mg/l) and 30 min (100 mg/l)).

Adsorption Isotherms and Thermodynamics

The adsorption isotherms were analyzed to understand the distribution of metal ions between the liquid and solid phases. The Langmuir model provided the best fit ($R^2 > 0.98$) for all three metals, indicating monolayer adsorption onto a homogeneous surface. The maximum monolayer adsorption capacities (q_{max}) for Pb(II), As(V), and Cd(II) at 303 K were calculated to be **480.07 mg/g**, **439.10 mg/g**, and **45.26 mg/g**, respectively. These values are significantly higher than those reported for many recent adsorbents, such as functionalized graphene oxides (Ahmad et al., 2020) and other CNT-based composites (Chandran et al., 2023), positioning our nanocomposite as a highly competitive material.

Thermodynamic analysis revealed negative ΔG° values, confirming the spontaneity of the adsorption process. The negative ΔH° values indicated an exothermic reaction, and the positive ΔS° values suggested an increase in randomness at the solid-solution interface during adsorption.

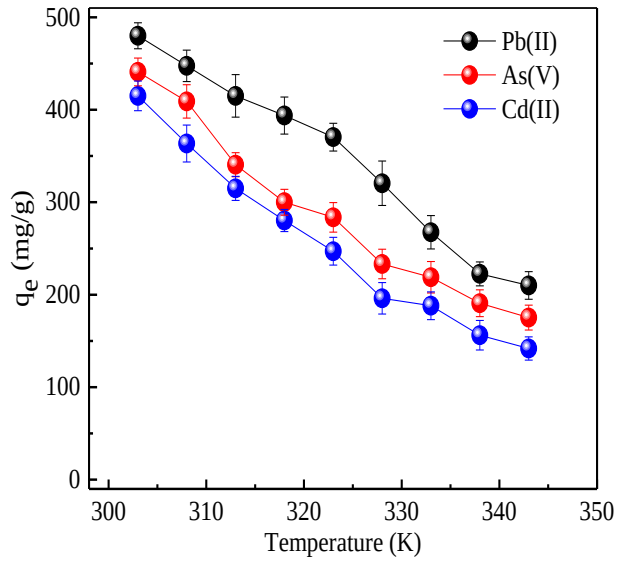

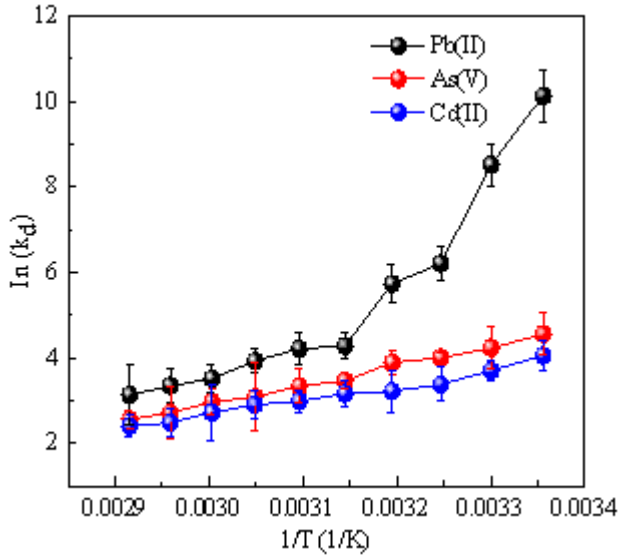

Figure 4.11 (a) Effect of temperature on metal ions adsorption by at pH (5), adsorbent dosage (43 mg/L) and contact time (30 min) and (b) the plot of ln(k_d) against 1/T;

To further understand the nature of the sorption process, the thermodynamic parameters for As(V), Cd(II) and Pb(II) adsorption on of MWCNTs-$ZnCl_2$@NiNP.were estimated by the fitted data shown in Fig.4.11b. The evaluated thermodynamic parameters such as, Gibbs free energy (ΔG°), enthalpy change (ΔH°) and entropy change (ΔS°) are presented in Table 4.4.

Table 4.4
Thermodynamic parameters for the adsorption of Pb(II), As(V) and Cd(II) by of MWCNTs-$ZnCl_2$@NiNP.composite.

Adsorbate	Temperature (K)	303	308	313	318	323	328	333	338	343
Pb(II)	ΔG° (kJ/mol)	-20.454	-15.888	-14.907	-12.304	-11.310	-10.698	-9.719	-9.398	-8.914
	ΔH° (kJ/mol)	-123.676								
	ΔS° (kJ/mol/K)	-0.342								
As(V)	ΔG° (kJ/mol)	-10.647	-10.249	-10.104	-9.144	-8.982	-8.398	-8.219	-7.635	-7.298
	ΔH° (kJ/mol)	-37.420								
	ΔS° (kJ/mol/K)	-0.087								
Cd(II)	ΔG° (kJ/mol)	-9.324	-8.643	-8.370	-8.355	-8.034	-7.912	-7.531	-6.88	-6.845
	ΔH° (kJ/mol)	-28.815								
	ΔS° (kJ/mol/K)	-0.063								

It can be seen that the values of ΔG°, ΔH° and ΔS° were all negative. Thus, the negative value of ΔG° reveals the viability of the adsorption process and the spontaneity of As(V)/Cd(II)/Pb(II) ions sorption on the surface ofIt can be seen that the values of ΔG°, ΔH° and ΔS° were all negative. Thus, the negative value of ΔG° reveals the viability of the adsorption process and the spontaneity of As(V)/Cd(II)/Pb(II) ions sorption on the surface of It can be seen that the values of ΔG°, ΔH° and ΔS° were all negative. Thus, the negative value of ΔG° reveals the viability of the adsorption process and the spontaneity of As(V)/Cd(II)/Pb(II) ions sorption on the surface of It can be seen that the values of ΔG°, ΔH° and ΔS° were all negative. Thus, the negative value of ΔG° reveals the viability of the adsorption process and the spontaneity of As(V)/Cd(II)/Pb(II) ions sorption on the surface ofMWCNTs-$ZnCl_2$@NiNP. In addition, the negative value of ΔH° validates the exothermic behavior of the current adsorption process, revealing that the adsorption capacity will decrease as temperature increases. Then again, negative value of ΔS° demonstrates reduction in randomness at the solid-liquid interface (Bhaumik *et al*., 2020). In all, the thermodynamic results showed strong corroboration with the results of adsorption kinetics.

In addition, the negative value of ΔH° validates the exothermic behavior of the current adsorption process, revealing that the adsorption capacity will decrease as temperature increases. Then again, negative value of ΔS° demonstrates reduction in randomness at the solid-liquid interface (Bhaumik *et al*., 2020). In all, the thermodynamic results showed strong corroboration with the results of adsorption kinetics.

CONCLUSION

This study successfully demonstrates the fabrication of a novel MWCNTs-$ZnCl_2$@NiNPs nanocomposite via a green and ultrasonication-assisted route. The composite exhibited exceptional adsorption performance for Pb(II), As(V), and Cd(II) ions, outperforming its individual components. The synergistic combination of the high-surface-area, porous MWCNT scaffold and the well-dispersed Ni nanoparticles resulted in high adsorption capacities, rapid kinetics, and excellent stability. The adsorption process was found to be spontaneous, exothermic, and best described by the PSO kinetic and Langmuir isotherm models. The incorporation of additional time points in the kinetic study provided a more detailed and reliable analysis of the adsorption mechanism. Given its high efficiency, eco-friendly synthesis, and magnetic separability, the MWCNTs-$ZnCl_2$@NiNPs composite presents a scalable and sustainable solution for the remediation of heavy metal-laden industrial wastewater, contributing significantly to the application of nanotechnology in environmental protection.

Declaration of Competing Interest

The authors acknowledge the sponsorship by TETFUND.

REFERENCES

Ahmad, S. Z. N., et al. (2020). Adsorptive removal of heavy metal ions using graphene-based nanomaterials. Chemosphere, 248, 126008.

Al-Kadhi, N. S., et al. (2022). Preparation of NiO/MWCNTs nanocomposite for the removal of cadmium ions. Journal of Materials Research and Technology, 19, 1961-1971.

Alsawy, T., et al. (2022). A comprehensive review on the chemical regeneration of biochar adsorbent for sustainable wastewater treatment. NPJ Clean Water, 5(1), 1. Chandran, D. G., et al. (2023). A review on adsorption of heavy metals from wastewater using carbon nanotube and graphene-based nanomaterials. Environmental Science and Pollution Research, 30(51), 110010-110046.

Egbosiuba, T. C., et al. (2022). Activated multi-walled carbon nanotubes decorated with zero valent nickel nanoparticles for arsenic, cadmium and lead adsorption from wastewater. Journal of Hazardous Materials, 423, 126993.

El Messaoudi, N., et al. (2024). Regeneration and reusability of non-conventional low-cost adsorbents. Biomass Conversion and Biorefinery, 14(11), 11739-11756. Gkika, D. A., et al. (2022). Why reuse spent adsorbents? The latest challenges and limitations. Science of The Total Environment, 822, 153555.

Gupta, K., et al. (2021). Recent advances in adsorptive removal of heavy metal and metalloid ions by metal oxide-based nanomaterials. Coordination Chemistry Reviews, 445, 214070.

Han, X., et al. (2024). Nickel Nanoparticles Encapsulated in N-Doped Carbon Nanotubes for Microwave Absorption. ACS Applied Nano Materials, 7(3), 2593-2604.

.Islam, Md & Hasan, Mehedi & Rahman, Mustafizur & Mobarak, Md Hosne & Mimona, Mariam Akter & Hossain,

Michael Chika Egwunyenga, et al (2023). Synthesis of Zero Valent Nickel Nano Biochar Composites from Guava Leaf Extract for the Adsorption of Heavy Metals from Wastewater, Journal of Water Resources and Pollution Studies,8(2), 1-9.

Nayem. (2024). Advances and significances of carbon nanotube applications: A comprehensive review. European Polymer Journal. 220. 113443. 10.1016/j.eurpolymj.2024.113443.

Kim, T. H., et al. (2022). Fabrication of Multi-Vacancy-Defect MWCNTs. Polymers, 14(5), 1020.

Rathinavel, S., et al. (2021). A review on carbon nanotube: An overview of synthesis, properties, functionalization, characterization, and the application. Materials Science and Engineering: B, 268, 115095.Ray, S., & Vashishth, R. (2024). Assessing the risk of consuming fish from Kanyakumari. Toxicology Reports.

Sable, H., et al. (2024). Strategically engineering advanced nanomaterials for heavy-metal remediation. Coordination Chemistry Reviews, 518, 216079.

Shrestha, Sabita & Bhatta, Jay. (2020). Simple Wet Chemical Route for Decoration of Multi-walled Carbon Nanotubes with Nickel Nanoparticles. Journal of Institute of Science and Technology. 25. 107-112. 10.3126/jist.v25i2.33746.

Ungureanu, Elena & Mustatea, Gabriel. (2022). Toxicity of Heavy Metals. 10.5772/intechopen.102441.

Wang, Z., et al. (2021). The selective adsorption performance and mechanism of multiwall magnetic carbon nanotubes for heavy metals in wastewater. Scientific Reports, 11, 16878. Zhang, T., et al. (2020). Removal of heavy metals and dyes by clay-based adsorbents. Chemical Engineering Journal, 420, 127574.

APPENDIX A

Percentage of PB(II) removal

Adsorbent dosage (mg/L)	MWCNTs-$ZnCl_2$@NINPs (%)	MWCNTs-$ZnCl_2$ (%)	NINPS (%)
5	58.20	40.50	31.20
10	62.50	50.80	33.40
15	66.80	57.50	42.40
20	70.50	60.50	49.20
25	82.50	61.20	51.30
30	94.20	61.40	51.20

Percentage of As(V) removal

Adsorbent dosage (mg/L)	MWCNTs-$ZnCl_2$@NINPs (%)	MWCNTs-$ZnCl_2$ (%)	NINPS (%)
5	57.30	40.62	22.80
10	60.20	50.10	27.60
15	70.10	52.10	30.42
20	77.70	55.13	33.30
25	82.60	61.30	42.61
30	90.80	61.80	43.93

Percentage of Cd(ii) removal

Adsorbent dosage (mg/L)	MWCNTs-$ZnCl_2$@NINPs (%)	MWCNTs-$ZnCl_2$ (%)	NINPS (%)
5	43.10	23.10	13.0
10	45.20	30.56	22.90
15	52.30	37.25	30.20
20	68.52	40.12	31.90
25	75.33	43.14	32.10
30	80.13	50.10	40.08

APPENDIX B

Contact Time(mins)	Adsorption capacity Pb(II) (mg/g)	Adsorption capacity As(II) (mg/g)	Adsorption capacity Cd(II) (mg/g)
20	423.05	378.23	345.76
40	489.23	440.63	410.23

60	488.90	448.53	408.10
120	488.92	445.83	410.10

Table 1: Adsorbate concentration: 100 mg/L

Time(mins)	Pb(II) (mg/g)	As(II) (mg/g)	Cd(II) (mg/g)
20	325.10	252.70	220.60
40	382.43	351.10	290.62
60	387.85	351.07	289.63
120	387.20	353.45	303.31

Table 2: Adsorbate concentration: 60 mg/L

Time(mins)	Pb(II) (mg/g)	As(II) (mg/g)	Cd(II) (mg/g)
20	182.60	378.10	103.02
40	231.05	202.12	156.23
60	253.62	209.57	176.35
120	255.61	210.75	169.23

Table 3: Adsorbate concentration : 20 mg/L